Tissue Engineering

Tissue Engineering Manuscript Central: http://mc.manuscriptcentral.com/ten

Bone regeneration mediated by a bioactive and biodegradable ECM-like hydrogel based on elastin-like recombinamers

Journal:	*Tissue Engineering*
Manuscript ID	TEA-2017-0047.R1
Manuscript Type:	Original Article
Date Submitted by the Author:	03-Mar-2017
Complete List of Authors:	Coletta, Dante; Universidad Nacional de Rosario, LABOATEM. Osteoarticular Biology, Tissue Engineering and Emerging Therapies Laboratory Ibáñez-Fonseca, Arturo; Universidad de Valladolid, BIOFORGE Lab Missana, Liliana; Universidad Nacional de Tucuman; Planta Piloto de Procesos Industriales Microbiologicos Jammal, María; Universidad Nacional de Tucuman; Planta Piloto de Procesos Industriales Microbiologicos Vitelli, Ezequiel; Universidad Nacional de Rosario, LABOATEM. Osteoarticular Biology, Tissue Engineering and Emerging Therapies Laboratory Aimone, Mariangeles; Universidad Nacional de Rosario, LABOATEM. Osteoarticular Biology, Tissue Engineering and Emerging Therapies Laboratory Zabalza, Facundo; Universidad Nacional de Rosario, LABOATEM. Osteoarticular Biology, Tissue Engineering and Emerging Therapies Laboratory Issa, João; Universidade de Sao Paulo, Ribeirão Preto School of Dentistry Alonso, Matilde; Universidad de Valladolid, BIOFORGE Lab Rodríguez-Cabello, José Carlos; Universidad de Valladolid, BIOFORGE Lab Feldman, Sara; Universidad Nacional de Rosario, LABOATEM. Osteoarticular Biology, Tissue Engineering and Emerging Therapies Laboratory
Keyword:	Bone < Applications in Tissue Engineering (DO NOT select this phrase; it is a header ONLY), Hydrogels < Enabling Technologies in Tissue Engineering (DO NOT select this phrase; it is a header ONLY), Biomimetics < Enabling Technologies in Tissue Engineering (DO NOT select this phrase; it is a header ONLY)
Manuscript Keywords (Search Terms):	bone regeneration, elastin-like recombinamers, bioactive hydrogels, BMP-2
Abstract:	The morbidity of bone fractures and defects is steadily increasing due to changes in the age pyramid. As such, novel biomaterials that are able to promote the healing and regeneration of injured bones are needed in order to overcome the limitations of auto-, allo-, and xenografts, while providing a ready-to-use product that may help to minimize surgical invasiveness

For Peer Review Only

and duration. In this regard, recombinant biomaterials, such as elastin-like recombinamers (ELRs), are very promising as their design can be tailored by genetic engineering, thus allowing scalable production and batch-to-batch consistency, amongst others. Furthermore, they can self-assemble into physically cross-linked hydrogels above a certain transition temperature, in this case body temperature, but are injectable below this temperature, thereby markedly reducing surgical invasiveness. Herein we have developed two bioactive hydrogel-forming ELRs, one including the osteogenic and osteoinductive BMP-2 and the other the RGD cell-adhesion motif. The combination of these two novel ELRs results in a BMP-2-loaded extracellular matrix-like hydrogel. Moreover, elastase-sensitive domains were included in both ELR molecules, thereby conferring biodegradation as a result of enzymatic cleavage and avoiding the need for scaffold removal after bone regeneration. Both ELRs and their combination showed excellent cytocompatibility, and the culture of cells on RGD-containing ELRs resulted in optimal cell adhesion. In addition, hydrogels based on a mixture of both ELRs were implanted in a pilot study involving a femoral bone injury model in New Zealand White rabbits, showing complete regeneration in six out of seven cases, with the other showing partial closure of the defect. Moreover, bone neo-formation was confirmed using different techniques, such as radiography, computed tomography and histology. This hydrogel system therefore displays significant potential in the regeneration of bone defects, promoting self-regeneration by the surrounding tissue with no involvement of stem cells or osteogenic factors other than BMP-2, which is released in a controlled manner by elastase-mediated cleavage from the ELR backbone.

SCHOLARONE™
Manuscripts

For Review Only Not for Distribution

For Peer Review ONLY/Not for Distribution

Bone regeneration mediated by a bioactive and biodegradable ECM-like hydrogel based on elastin-like recombinamers

Dante J. Coletta, MD,[1#] Arturo Ibáñez-Fonseca, MSc,[2#] Liliana R. Missana, PhD,[3,4#] María V. Jammal, PhD,[3,4] Ezequiel J. Vitelli, MD,[1] Mariangeles Aimone, BSc,[1] Facundo Zabalza, BSc,[1] João P. Mardegan Issa, PhD,[5] Matilde Alonso, PhD,[2] José Carlos Rodríguez-Cabello, PhD,[2] and Sara Feldman, PhD[1]

[#] These authors contributed equally to this work.

[1] LABOATEM. Osteoarticular Biology, Tissue Engineering and Emerging Therapies Laboratory, School of Medicine, National Rosario University, Rosario, Argentina.

[2] BIOFORGE Lab, University of Valladolid, CIBER-BBN, Valladolid, Spain.

[3] Experimental Pathology & Tissue Engineering Laboratory, Dental School, National Tucumán University, Tucumán, Argentina.

[4] Tissues Laboratory, Proimi-Biotechnology-Conicet, Tucumán, Argentina.

[5] Ribeirão Preto School of Dentistry, University of São Paulo, São Paulo, Brazil.

Address correspondence to:

José Carlos Rodríguez-Cabello, PhD

BIOFORGE Lab

Universidad de Valladolid

Paseo de Belén, 19

47011 – Valladolid

SPAIN

E-mail: roca@bioforge.uva.es

Phone: +34983184585

Abstract

The morbidity of bone fractures and defects is steadily increasing due to changes in the age pyramid. As such, novel biomaterials that are able to promote the healing and regeneration of injured bones are needed in order to overcome the limitations of auto-, allo-, and xenografts, while providing a ready-to-use product that may help to minimize surgical invasiveness and duration. In this regard, recombinant biomaterials, such as elastin-like recombinamers (ELRs), are very promising as their design can be tailored by genetic engineering, thus allowing scalable production and batch-to-batch consistency, amongst others. Furthermore, they can self-assemble into physically cross-linked hydrogels above a certain transition temperature, in this case body temperature, but are injectable below this temperature, thereby markedly reducing surgical invasiveness. Herein we have developed two bioactive hydrogel-forming ELRs, one including the osteogenic and osteoinductive BMP-2 and the other the RGD cell-adhesion motif. The combination of these two novel ELRs results in a BMP-2-loaded extracellular matrix-like hydrogel. Moreover, elastase-sensitive domains were included

For Peer Review ONLY! Not for Distribution

in both ELR molecules, thereby conferring biodegradation as a result of enzymatic cleavage and avoiding the need for scaffold removal after bone regeneration. Both ELRs and their combination showed excellent cytocompatibility, and the culture of cells on RGD-containing ELRs resulted in optimal cell adhesion. In addition, hydrogels based on a mixture of both ELRs were implanted in a pilot study involving a femoral bone injury model in New Zealand White rabbits, showing complete regeneration in six out of seven cases, with the other showing partial closure of the defect. Moreover, bone neo-formation was confirmed using different techniques, such as radiography, computed tomography and histology. This hydrogel system therefore displays significant potential in the regeneration of bone defects, promoting self-regeneration by the surrounding tissue with no involvement of stem cells or osteogenic factors other than BMP-2, which is released in a controlled manner by elastase-mediated cleavage from the ELR backbone.

Keywords: bone regeneration, elastin-like recombinamers, bioactive hydrogels, BMP-2.

Introduction

It is well known that dental, maxillofacial, and other orthopedic surgeries often require the use of different biomaterials for the treatment of injuries and other diseases through tissue engineering, including osteoporosis (1-6). In addition, changes of the age pyramid towards an older population have led to an increasing number of bone fractures (7-11). Despite the availability of numerous biomaterials for tissue regeneration, autologous bone is usually the first option for the replacement of injured bone tissue. However, a large number of different types of biomaterials and bone grafts have been employed to date for the healing of bone defects (12). These biomaterials should be: a)

For Peer Review ONLY/Not for Distribution

osteoinductive, hence promoting stem cell differentiation to osteoblasts, b) osteoconductive, thereby inducing growth of the surrounding healthy bone, and c) osseointegrative, merging with the nearby bone (13-15). They should also stimulate an optimal cell response and be liable to be replaced by *de novo* formed tissue, acting as a provisional substitute (1, 16, 17).

Engineered biomaterials, in combination with growth factors, have been shown to be an effective approach in bone tissue engineering since they can act both as a scaffold and as a drug-delivery system to promote bone repair and regeneration (18, 19). For instance, the osteoinductive bone morphogenetic protein-2 (BMP-2) (20, 21) has been shown to enhance the formation of bone tissue in situations that lead to bone degradation, such as alcohol dependence (22) and osteometabolic diseases (23). Due to the high cost and rapid release of BMP-2 when placed at the site of injury, it is often associated with carrier matrices that act as drug-delivery systems to increase its half-life and to avoid the adverse effects associated to high doses of BMP-2 (24-27).

On the other hand, protein-based recombinant biomaterials, such as resilin-, silk-, collagen- and elastin-like polypeptides, have been developed over the last few decades with the aim of improving the features of traditional biomaterials in terms of ease of design and synthesis, biocompatibility and bioactivity (28). As an example, elastin-like recombinamers (ELRs), thus named due to their polymeric and recombinant nature (29), have been shown to be a potential tool for the development of biomedical devices for regenerative medicine due to their thermosensitivity. This smart behavior is a result of their composition, which is based on repetitions of the Val-Pro-Gly-X-Gly (VPGXG) pentapeptide, in which X (guest residue) is any amino acid except L-proline. Moreover, it is characterized by a transition temperature (T_t) which itself depends on the polarity of the side chain in the guest residue. Thus, in an aqueous medium, the ELR chains remain

For Peer Review ONLY/Not for Distribution

soluble below their T_t while above that T_t (e.g. physiologic temperature) the ELR self-assembles hydrophobically, undergoing a phase transition (30). In this study, two different ELRs have been developed, based on a previously described hydrogel-forming ELR (31). Taking advantage of the recombinant nature of these biomolecules, one of the novel ELRs designed in this work has been genetically engineered to include Arg-Gly-Asp (RGD) motifs to enhance cell adhesion via cell-membrane integrins (32), whereas the other ELR was designed to include BMP-2. Both ELRs also contain elastase-sensitive domains resulting from repetition of the VGVAPG hexapeptide (33) to improve the enzymatic biodegradability of the biomaterial.

In order to study the potential of these novel ELRs in bone regeneration, we have used a previously developed model of femoral bone injury (FBI) in New Zealand White rabbits. This involves the creation of a defect 6 mm in diameter in a femoral condyle 8 mm in diameter (34, 35). This animal model allows the study of the defect by computed tomography (CT) and by radiological studies given the size of the bone.

The aim of this work was to evaluate whether novel bioactive ELRs are cytocompatible and degradable, while being able to form extracellular matrix (ECM)-like hydrogels and promoting bone regeneration after implantation into an FBI in rabbits, as a preliminary step for their use in humans. For this purpose, the cytocompatibility and biodegradation ability were assessed *in vitro*, and a highly reproducible model was subsequently used to carry out a pilot *in vivo* study.

Materials and methods

Ethical approval

Experimental procedures regarding the use of animals were approved by the Bioethics Committee of Rosario National University (Resolution No. 150/2015). Its regulations

For Peer Review ONLY/Not for Distribution

include well-established guidelines for animal care and manipulation to decrease pain and suffering of the animal, according to the 3Rs (replacement, reduction and refinement), and are in accordance with international laws concerning the use of animals.

ELR biosynthesis and characterization

The genetic construction of the ELRs used in this work was performed as described elsewhere (36). Briefly, their DNA sequences were obtained by genetic engineering techniques and cloned into a pET-25b(+) vector for expression in *Escherichia coli*. ELRs were biosynthesized in a 15-L bioreactor and purified by several cooling and heating purification cycles (Inverse Transition Cycling) taking advantage of the ability of these recombinamers to precipitate above their transition temperature. Further centrifugation steps led to a pure product, which was dialyzed against ultra-pure water, filtered through 0.22 μm filters (Nalgene, Thermo Fisher, USA) to obtain a sterile solution, and freeze-dried prior to storage. The ELRs were found to contain less than two endotoxin units (EU)/mg of ELR, as determined using the limulus amebocyte lysate assay with the Endosafe®-PTS system (Charles River Laboratories). This process allowed the production of two different ELRs, both of which were derived from a previously synthesized block co-recombinamer (31). Further information can be obtained in Supplementary Methods (Supplementary Information).

The characterization techniques used included sodium dodecyl sulfate polyacrylamide gel electrophoresis (SDS-PAGE) and matrix-assisted laser desorption/ionization time-of-flight (MALDI-TOF) spectrometry for purity and molecular weight (*Mw*) evaluation compared to the theoretical values of 113,556 Da for ELR-E-RGD and 107,752 Da for ELR-E-BMP-2; differential scanning calorimetry (DSC) to determine the transition

For Peer Review ONLY/Not for Distribution

temperature; HPLC to determine the amino acid composition of both ELRs (Table S1 and Table S2, Supplementary Information), and nuclear magnetic resonance (NMR) to provide recombinamer fingerprint data (Fig. S3 and S4; Table S3 and Table S4, Supplementary Information). The procedure for the measurement of the mechanical properties of ELR-based hydrogels is described in Supplementary Methods (Supplementary Information).

Elastase-mediated cleavage of the ELR in solution

Different quantities (1.2, 1.8 and 2.4 U) of porcine pancreas elastase (4 mg/mL, 6.8 U/mg) (Sigma-Aldrich, USA) were added to solutions of the mixture of both ELRs (98% (w/w) ELR-E-RGD and 2% (w/w) ELR-E-BMP-2) at a final concentration of 1 mg/mL dissolved in ultra-pure water in order to evaluate the biodegradation rate for each quantity of enzyme. The quantity of elastase used was 2000-, 3000- and 4000-times the amount needed to cleave the mixture of ELRs used as substrate in 30 minutes, since preliminary experiments showed that larger quantities than those calculated are required to observe an actual effect of the enzyme *in vitro*. Samples were incubated at 37 ºC and collected at various time points (10, 20, 30, 45, 60, 90 and 120 minutes), then stored frozen at –20 ºC until further use. A negative control, namely an ELR molecule lacking elastase-sensitive sequences but with the same elastin-like structure as the two ELRs designed for this work (31), was also treated with 1.2 U of elastase for further comparisons. Methods concerning the evaluation of the biodegradation are explained in Supplementary Methods (Supplementary Information).

In vitro *cell culture*

Bone marrow derived human mesenchymal stem cells (hMSCs) were extracted and isolated as described elsewhere (37) and were generously provided as a gift by Citospin

For Peer Review ONLY/Not for Distribution

S.L. (Spain). They were cultured for expansion in DMEM low glucose (1 g/L) (Gibco, USA) supplemented with 10% fetal bovine serum (FBS) (Gibco, USA) and 1% Penicillin/Streptomycin (P/S) (Gibco, USA).

All cells were used at passage 3-5 in subsequent experiments. They were detached from the wells using a Trypsin-EDTA solution (0.25%, Gibco, USA) and counted using a hematocytometer.

Cell viability

Human MSCs were used to determine the *in vitro* viability using the Calcein AM assay (Molecular Probes, USA) when cultured in DMEM supplemented with 10 mg/mL of the different ELRs or the mixture of them (98% (w/w) ELR-E-RGD and 2% (w/w) ELR-E-BMP-2) for 3 days. This assay was performed in a black, 96-well plate with clear-bottom (Greiner Bio One, USA) according to the manufacturer's instructions and the fluorescence intensity measured at 530 nm using a plate reader (SpectraMax M2e, Molecular Devices, USA). The intensity measured at this wavelength, corresponding to live cells, was then used to calculate cell numbers by using calibration curves obtained with different known quantities of cells (from 1000 to 10,000 cells per well) seeded on 96-well plates 24 h before the measurement. Each condition was performed in triplicate, with four experiments for each (n = 4).

Cell adhesion on ELR-coated tissue culture plates

96-well plates were used for the coating of different wells with both ELRs separately and combined (98% (w/w) ELR-E-RGD and 2% (w/w) ELR-E-BMP-2). Briefly, a 5 mg/mL solution of the recombinamers in ultra-pure water was placed in the well and allowed to adsorb to the surface for 24 h at 4 ºC. The wells were washed twice with 1x PBS (Gibco) and blocked with 1% BSA for 2 h at 37 ºC, then rinsed again and, finally,

For Peer Review ONLY / Not for Distribution

3000 cells per well were seeded onto the modified surfaces to study cell adhesion after 24 hours. The number of cells in each well was determined using the Calcein AM assay as described above.

Dissolution of the ELRs for the in vivo *experiments*

A mixture of both ELRs (98% (w/w) ELR-E-RGD and 2% (w/w) ELR-E-BMP-2) was prepared and dissolved in sterile tubes (one per animal) at 300 mg/mL with 1x sterile phosphate buffered saline (PBS) (Gibco, USA) by incubation at 4 ºC for 24 h. A 2% (w/w) ELR-E-BMP-2 solution at 300 mg/mL gives a similar amount of BMP-2 in our device ($5.57 \cdot 10^{-5}$ M) as in INFUSE® Bone Graft ($5.77 \cdot 10^{-5}$ M, Medtronic, USA) (38). This solution was kept in an ice bath during surgery until implantation.

In vivo *experiments*

Adult female New Zealand white rabbits (n = 7) with an average weight of 3.5 kg were used for the creation and treatment of bone defects. These animals were kept in individual cages with food (ACA Cooperativas, Argentina) and water *ad libitum*.

Antibiotic prophylaxis, anesthetic treatment and surgical techniques were performed according to a previously described procedure (34, 35). Further details regarding the surgical procedure can be found in Supplementary Methods (Supplementary Information). Three months post-surgery, the animals were euthanized using three doses of anaesthesia, as previously described (34, 39). The femora were then collected to perform different experiments to assess bone regeneration (see below).

Multi-slice computed tomography (MSCT)

Multi-slice computed tomography was performed on the seven right femurs of the rabbits using a Toshiba Alexion apparatus with 16 detectors and a thickness of 0.5 mm.

For Peer Review ONLY, Not for Distribution

For Peer Review ONLY/Not for Distribution

Coronal, sagittal and axial slices were obtained and the images were processed using Alexion Advance Edition software with the Adaptive Iterative Dose Reduction (AIDR 3D) algorithm, thus obtaining the 3D reconstruction for every sample. All images were analyzed together for an optimal comparison.

Bone histopathology

Femoral bone samples were evaluated by way of radiographic studies using a conventional dental X-ray machine with dental occlusal films (Eastman Kodak, USA) to determine the implant position to guide the histological procedures. The femoral epiphysis was cut 4 cm below the metaphysis using a carborundum-disk cutter (Dochem, China) attached to a dental drill under irrigation with distilled water. The implanted area was marked with Indian ink. Two samples were selected for decalcification using modified Morse solution (Okayama University Dental School) and embedded in paraffin following well-established protocols. The samples were serial cut (7 μm thick) using a manual rotary microtome (Micron-Zeiss, Germany), and stained with Hematoxylin & Eosin (H&E). All specimens were examined by light microscopy and evaluated by a single pathologist. Subsequently, another pathologist (certified by the Argentinean Ministry of Health No. 31455) performed an independent review to verify microscopic observations. The reported results reflect the mutually-agreed-upon diagnoses by both pathologists. Photomicrographs were taken from slides of each specimen using a Sony digital camera fitted to an Olympus CH30 microscope with an Olympus stereo zoom SZ51.

Statistical analysis

Data for the *in vitro* experiments are reported as mean ± SD (n = 4). Statistical analysis of data following a normal distribution was performed using a one-way analysis of

variance and the Holm–Sidak method. A p-value of less than 0.05 was considered to be statistically significant, while $p > 0.05$ indicates no significant differences (n.s.d.). (*) $p < 0.05$, (**) $p < 0.01$.

Results

ELR Biosynthesis and characterization

Both ELRs were obtained as a lyophilized product in a yield of approximately 200 mg/L (ELR/culture volume). Their molecular weights and purities were confirmed as satisfactory by SDS-PAGE and MALDI-TOF (Fig. 1), while the T_t calculated by DSC for the ELRs dissolved in PBS (pH 7.4) was found to be 15.8 ºC and 15.3 ºC for ELR-E-RGD and ELR-E-BMP-2, respectively (Fig. S2, Supplementary Information).

As regards the mechanical characterization, the storage modulus (G') of the ELR-based hydrogel at a concentration of 300 mg/mL (98% ELR-E-RGD and 2% ELR-E-BMP-2) was found to be approximately 1600 Pa at 37ºC (Fig. S5, Supplementary Information). In addition, hydrogels were formed above the T_t, as observed macroscopically (Fig. S6, Supplementary Information).

Enzymatic cleavage of ELR molecules by elastase digestion

Due to the incorporation of elastase-sensitive domains in the ELR molecules designed for this work, we aimed to verify whether elastase was able to cleave these ELRs. Hence, a mixture of them (98% ELR-E-RGD and 2% ELR-E-BMP-2) was dissolved at 1 mg/mL, and ELRs were found to be cleaved *in vitro* in solution when different quantities of elastase were added. As observed in Fig. 2, and as expected, the ELRs are sensitive to the quantity of elastase, therefore biodegradation was slower when only 1.2 U of elastase was added to the ELR solution (Fig. 2a), whereas an increase in the

For Peer Review ONLY/Not for Distribution

biodegradation rate was observed if 1.8 U (Fig. 2b) or 2.4 U (Fig. 2c) of elastase were supplemented. In contrast, no elastase-mediated cleavage was observed in the negative control at any sample collection time (Fig. 2d).

The disappearance of the larger bands at 113.6 and 107.8 kDa was further studied by image analysis, and the results are summarized in Fig. 3. This figure clearly reinforces the statement made above regarding the biodegradation rate, namely that biodegradation is faster as more elastase is added to the solution.

As regards the nascent bands observed by SDS-PAGE (Fig. 2), we expected to obtain bands in three different molecular weight ranges, namely 65.5-66.5, 46.7-48.2, and 12-12.9 kDa, as by-products of ELR-E-RGD/BMP-2 digestion since there are two different elastase-sensitive domains at different points in the ELR-E-BMP-2 molecule. However, the molecular weight of the higher bands was found to be 80.8 and 54.2 kDa, respectively, while the band at 12-12.9 kDa could not be observed due to the limitations of SDS-PAGE in terms of resolution. Nevertheless, these results correlate well with previous studies that reported a 20% increase in the apparent molecular weight for different ELRs (40, 41). As such, we estimated the *Mw* plus 20% and the values showed good agreement with those found empirically, with the experimental values for the nascent bands being 80.8 and 54.2 kDa, while the expected values of *Mw* + 20% were 78.6-79.8 and 56.0-57.8, respectively (Table S5, Supplementary Information).

hMSCs viability and integrin-mediated cell adhesion

The viability of the cells after culture for 3 days in media supplemented with the ELRs was found to be similar to that for the negative control, i.e. medium without supplementation, as can be observed in Fig. 4. Since no significant differences were

For Peer Review ONLY/Not for Distribution

observed, we can conclude that the ELRs alone, or the mixture thereof, do not affect cell viability.

Furthermore, the evaluation of cell adhesion in ELR-coated tissue culture plates (TCP) showed good results in the case of ELR-E-RGD and the mixture of both. This finding was in agreement with our expectations since the mixture contains 98% ELR-E-RGD. However, coating only with ELR-E-BMP-2 led to statistically significantly lower levels of attachment due to the lack of cell-adhesion domains in the recombinamer (Fig. 5).

Biochemical and clinical results

The welfare of the animals in the first two days post-implantation was slightly affected, with disrupted walking, as expected. After seven days, treated animals behaved similarly to their non-operated control counterparts. The temperature values, food intake and all the biochemical parameters measured were similar between animals from control groups at every time point studied (n.s.d., $p > 0.05$).

MSCT studies

MSCT studies showed bone healing in the defect area. A closer examination of the distal metaepiphysis region, in the medial cortical plane, showed total closure of the defect in most of the coronal and sagittal slices for all of the samples analyzed. However, it was possible to identify the persistence of a small defect with a diameter of 1 mm in the medial cortical plane of the lesion site in one of the femora extracted, although only in one coronal slice and two axial ones (Fig. 6a and 6b, white arrow). These results were confirmed by radiological studies (Fig. S7, Supplementary Information).

Bone restitution in the distal femoral metaphysis was also observed in the 3D reconstructions of all samples, and the created defect could not be detected (injury site

For Peer Review ONLY! Not for Distribution

indicated with a black circle; Fig. 6c), even in the case of the sample that showed a small defect remaining in the axial and coronal slices. This 3D reconstruction showed a tiny hollow (white arrow), but the processed signal correlates to cortical bone (Fig. 6d).

Histopathology results

The histological analytical results obtained for experimental samples showed *de novo* bone formation in the experimental femoral injury (EFI) region. The new bone formed was thick and comprised lamellar bone. In addition, it showed numerous vascular channels of different calibers and was surrounded by various osteoblast layers (Fig. 7a). Each bone layer was deposited on the remaining ELR hydrogel in a disorganized fashion (Fig. 7b), resembling pagetoid-like bone (Fig. 7c), in which cellular activity produces a mosaic pattern rather than the normal linear lamellar pattern.

Remnants of non-biodegraded ELR hydrogels were observed inside the EFI center, showing a network or mesh shape and surrounded by micro-hemorrhages and congestive vessels. Rounded, triangular, rhomboid or even amorphous structures were found inside the network, showing an eosinophil, granular and mineralized pattern. These mineralized structures were surrounded by osteoblast-like cells, with osteocyte-like cells being found inside them, and angiogenesis could also be observed (Fig. 7d).

Hematopoietic bone marrow was observed surrounding the newly formed bone in the EFI, with scattered, rounded, nodule-like trabecular bone (Fig. 7e). This new trabecular bone was covered by two, three or even more layers of prominent osteoblasts. Osteocyte cells were observed in the inner region, (Fig. 7f). Furthermore, several congestive vessels were observed close to each trabecula.

For Peer Review ONLY/ Not for Distribution

For Peer Review ONLY/Not for Distribution

Discussion

In order to address the main aim of this work, namely the regeneration of a femoral bone injury (FBI) in three-year-old female New Zealand white rabbits, two different bioactive ELRs have been developed and characterized to meet the requirements of novel biomaterials commonly used for that purpose. These novel ELRs were specifically designed to be osteoinductive, by fusing BMP-2 to one of them, and osteoconductive, by fusing RGD domains that promote cell adhesion, thus allowing surrounding cells to interact with the hydrogel and possibly promote bone formation even from inside the scaffold.

Initially it was shown that the T_t is lower than body temperature, which may permit the formation of hydrogels once the ELR solution is injected into the body. In addition, this T_t is similar to that described previously for the non-bioactive ELR, which was found to be 13.0 ºC (42), although an increase of 2.8 and 2.3 ºC was observed for ELR-E-RGD and ELR-E-BMP-2, respectively. This can be explained by the lower hydrophobicity of the ELR molecule when other, more hydrophilic peptides or proteins containing charged residues are fused to it (43, 44).

As regards the rheological data, although this system is intended to be used for bone regeneration and the storage modulus is very low in comparison with bone tissue, this hydrogel was designed to be able to promote cell invasion and proliferation inside itself, acting as a temporary soft tissue that promotes optimal regeneration in a manner whereby the implanted scaffold is substituted by host tissue. As such, although it may not be useful on its own for treating large bone defects, it has been shown to be very suitable in the FBI model used in this work since the hydrogel remains free from significant mechanical stress (45).

Biodegradation of the ELR molecules in solution has been confirmed *in vitro*, thus showing that this process can also be controlled by varying the quantity of elastase used. Although this fails to imitate *in vivo* conditions, it sheds light onto the biodegradation kinetics. The use of elastase-sensitive sequences should also allow the slow release of BMP-2 from the ELR molecule to exert its biological effect. Consequently, the ELR-based hydrogel acts as a drug-delivery system. Despite the fact that there are other examples in which rhBMP-2 and ELRs are combined as an encapsulation system (46), this approach allows a more efficient production and application by taking advantage of recombinant DNA technology.

The excellent cell adhesion found on surfaces coated with ELR-E-RGD was similar to that obtained in other studies using RGD-containing ELRs (47). As such, this work demonstrates that the inclusion of RGD sequences in the final ELR molecule by genetic-engineering methods promotes cell attachment and therefore provides a more ECM-mimetic environment that is also osteoconductive. ELR-E-BMP-2-coated substrates did not support cell adhesion due to the absence of cell-adhesion motifs in the ELR itself and in BMP-2. With regard to cell viability, the lack of differences between the negative control (medium only) and the media supplemented with the recombinamers is in agreement with previous studies in which a cell-culture medium was supplemented with ELRs (48).

As regards the clinical and biochemical results of the implant process, although initially affected by the surgery *per se*, animal gait recovered rapidly to normal conditions. The lack of change in the biochemical parameters showed that neither the surgical procedure nor the subsequent possible matrix biodegradation had any effect on the animals, thus showing good biocompatibility.

For Peer Review ONLY/Not for Distribution

The images obtained in the tomographic study with 3D reconstruction of the samples show promising results since the signal patterns processed in this work are correlated to bone tissue with similar characteristics to the surrounding tissue, with complete closure of the defect being achieved in six out of seven samples. Although a defect approximately 1 mm in diameter was still visible in the remaining animal, this was only the case in three tomographic slices and may simply be a consequence of a lack of time for the regeneration process in this particular animal. However, the bone formed had the same characteristics as the other samples, therefore it can be concluded that these ELR-based matrices have a high osteogenic potential to restitute a bone defect of 6 mm diameter and 6 mm depth *ad integrum* in 90 days, most probably due to fusion of the BMP-2 protein to the ELR, which results in a BMP-2-loaded hydrogel.

The histological analyses showed that the FBI was replaced by dense, new lamellar bone. Although a few remnants of the ELR were observed at 90 days post-implantation, they were surrounded by congestive vessels and dense laminar bone. This supports the accepted knowledge whereby new bone is only formed in the presence of blood irrigation (49). This new bone is arranged randomly, with an irregular arrangement in various different directions, thus suggesting that the ELR-based hydrogels act as a carrier for BMP-2, with osteoprogenitor cells colonizing these hydrogels, depositing osteoid matrix and mineralizing as pagetoid-like bone, probably driven by the network arrangement of the ELR-based hydrogels (50). The new trabeculae obtained show a peculiar shape, as if they were obtained by the confluence of rounded isolated bone formations. The numerous layers of prominent osteoblasts and various shapes observed, which appear to simulate pseudo-stratification, could be a result of the activity of BMP-2 (22, 51, 52).

For Peer Review ONLY/Not for Distribution

As observed *in vivo* from the microscopic results, the ELR-based hydrogel was found to be biodegraded as bone formation occurred since the cells involved in this phenomenon were stimulated by the BMP-2 released into the microenvironment, probably slowly enough to allow the differentiation of stem and progenitor cells. As such, in this situation, elastase (MMP-12) secretion by osteoclasts might be increased as a consequence of matrix remodeling due to the formation of *de novo* bone tissue, as suggested before (53). This could lead to degradation of the ELR-based hydrogel, which is sensitive to MMP-12 as a result of inclusion of the VPVAPG sequence, as described previously (54). On the other hand, ELRs without cleavable domains are not supposed to be biodegraded. In this regard, Sallach *et al*. reported a long-term stability (up to 1 year) of a physically cross-linked ELR-based hydrogel, similar to the one used in our work, when implanted *in vivo* (55). In our case, biodegradation might happen simultaneously with bone regeneration, thus resulting in a resorbable matrix that maintains bone integrity until full regeneration. In addition, the peptides resulting from the degradation of VPVAPG have been reported to exhibit a strong cell-proliferation activity that may promote tissue repair, as described previously (56). Furthermore, RGD sequences provide anchoring points for cells that help them to migrate and proliferate inside the scaffold, thereby promoting self-regeneration of the damaged tissue.

Although several approaches have been developed in the field of tissue engineering, to the best of our knowledge this is the first work describing the use of ELR-based hydrogels for the successful regeneration of a bone defect *in vivo*. Previous examples make use of ELRs in combination with other materials (57, 58), and most of them have only been tested *in vitro*, although with promising results (59). Besides, the ELR-based hydrogel described in this study overcomes different issues regarding the use of biomaterials in bone tissue engineering. For instance, BMP-2 is not only loaded inside

For Peer Review ONLY! Not for Distribution

the hydrogel, but it is part of it. Hence, there is no need to add this osteogenic factor during the preparation of the scaffold, in contrast to other works (60), reducing its cost. In addition, this acellular system has shown to be able to promote optimal bone regeneration, while other studies report good outcomes only in the presence of mesenchymal stromal cells (61, 62). On the other hand, another acellular scaffold has been described, showing its usefulness in bone regeneration (63). However, this system is not injectable, and thus requires the use of invasive methods for its implantation. Moreover, the adaptation of this scaffold to the shape of the defect depends on the mold used in its development, reducing its versatility.

In conclusion, this work shows that a mixture of the originally designed ELRs is able to self-assemble into an appropriate BMP-2 carrier, namely an injectable and biodegradable hydrogel, which allows the slow release of this osteogenic factor, thereby stimulating progenitor and stem cell differentiation and osteoblast proliferation. Furthermore, the resulting ELR-based hydrogels also demonstrated an osteoconductive behavior since they provide an ECM-like environment as a result of the inclusion of RGD sequences. These two bioactivities (RGD and BMP-2), together with elastase-sensitiveness were easily included in the final ELR molecules in a controlled manner, due to their recombinant nature. Endogenous cells were able to migrate and proliferate into these hydrogels, thereby favouring bone neo-formation at the femoral injury, as confirmed by computed tomography, radiography and histology.

Acknowledgments

The authors are grateful for funding from the European Commission (NMP-2014-646075, HEALTH-F4-2011-278557, PITN-GA-2012-317306 and MSCA-ITN-2014-642687), the MINECO of the Spanish Government (MAT2013-42473-R and

For Peer Review ONLY/Not for Distribution

MAT2013-41723-R), the Junta de Castilla y León (VA244U13 and VA313U14) and the Centro en Red de Medicina Regenerativa y Terapia Celular de Castilla y León. Dante J. Coletta has been funded by the Consejo Nacional de Investigaciones de Ciencia y Tecnología de la Nación (CONICET, Argentina). We would also like to thank Dr. Pedro Esbrit, from the Jiménez Díaz Foundation.

Author Disclosure Statement

No competing financial interests exist.

References

1. Amini, A.R., Laurencin, C.T., and Nukavarapu, S.P. Bone Tissue Engineering: Recent Advances and Challenges. Critical reviews in biomedical engineering **40**, 363, 2012.

2. Khademhosseini, A., and Langer, R. A decade of progress in tissue engineering. Nat Protocols **11**, 1775, 2016.

3. Yoseph, B.-C. Biomimetics. Biomimetics: CRC Press; 2005. pp. 495.

4. Costa, H.S., Mansur, A.A.P., Pereira, M.M., and Mansur, H.S. Engineered Hybrid Scaffolds of Poly(vinyl alcohol)/Bioactive Glass for Potential Bone Engineering Applications: Synthesis, Characterization, Cytocompatibility, and Degradation. Journal of Nanomaterials **2012**, 16, 2012.

5. Santolini, E., West, R., and Giannoudis, P.V. Risk factors for long bone fracture non-union: a stratification approach based on the level of the existing scientific evidence. Injury **46 Suppl 8**, S8, 2015.

For Peer Review ONLY Not for Distribution

6. Chrcanovic, B.R., Albrektsson, T., and Wennerberg, A. Dental implants inserted in male versus female patients: a systematic review and meta-analysis. Journal of oral rehabilitation **42**, 709, 2015.

7. Cointry, G.R., Capozza, R.F., Feldman, S., Reina, P., and Ferretti, J.L. Estructura y biomecánica ósea. In: E. A., ed. Osteoporosis en Iberoamérica (2ª Ed). México DF (México): El Manual Moderno; 2012. pp. 33.

8. Compston, J. Osteoporosis: social and economic impact. Radiologic clinics of North America **48**, 477, 2010.

9. Curran, D., Maravic, M., Kiefer, P., Tochon, V., and Fardellone, P. Epidemiology of osteoporosis-related fractures in France: a literature review. Joint, bone, spine : revue du rhumatisme **77**, 546, 2010.

10. Cointry, G.R., Capozza, R.F., Feldman, S., Reina, P., Grappiolo, I., Ferretti, S.E., Mortarino, P., Chiappe, M.A., and Ferretti, J.L. Los huesos son estructuras genéticas, metabólicas, biomecánicas, o todo a la vez. Actualizaciones en Osteología **5**, 184, 2009.

11. Melton, L.J., 3rd, Achenbach, S.J., Atkinson, E.J., Therneau, T.M., and Amin, S. Long-term mortality following fractures at different skeletal sites: a population-based cohort study. Osteoporosis international : a journal established as result of cooperation between the European Foundation for Osteoporosis and the National Osteoporosis Foundation of the USA **24**, 1689, 2013.

12. Kremenetzky, A., Kremenetzky, L., and Feldman, S. Aplicación de aloinjerto óseo como cemento biológico. Revista de la Asociación Argentina de Ortopedia y Traumatología **71**, 61, 2006.

For Peer Review ONLY/Not for Distribution

13. Alghazali, K.M., Nima, Z.A., Hamzah, R.N., Dhar, M.S., Anderson, D.E., and Biris, A.S. Bone-tissue engineering: complex tunable structural and biological responses to injury, drug delivery, and cell-based therapies. Drug metabolism reviews **47**, 431, 2015.

14. Zhang, S., Zhang, X., Cai, Q., Wang, B., Deng, X., and Yang, X. Microfibrous beta-TCP/collagen scaffolds mimic woven bone in structure and composition. Biomedical materials **5**, 065005, 2010.

15. Arealis, G., and Nikolaou, V.S. Bone printing: new frontiers in the treatment of bone defects. Injury **46 Suppl 8**, S20, 2015.

16. Salgado, A.J., Oliveira, J.M., Martins, A., Teixeira, F.G., Silva, N.A., Neves, N.M., Sousa, N., and Reis, R.L. Chapter One - Tissue Engineering and Regenerative Medicine: Past, Present, and Future. In: Stefano Geuna I.P.P.T., Bruno B., eds. International Review of Neurobiology: Academic Press; 2013. pp. 1.

17. Detsch, R., and Boccaccini, A.R. The role of osteoclasts in bone tissue engineering. Journal of tissue engineering and regenerative medicine **9**, 1133, 2015.

18. van der Stok, J., Lozano, D., Chai, Y.C., Amin Yavari, S., Bastidas Coral, A.P., Verhaar, J.A.N., Gómez-Barrena, E., Schrooten, J., Jahr, H., Zadpoor, A.A., Esbrit, P., and Weinans, H. Osteostatin-Coated Porous Titanium Can Improve Early Bone Regeneration of Cortical Bone Defects in Rats. Tissue Engineering Part A **21**, 1495, 2015.

19. Romagnoli, C., D'Asta, F., and Brandi, M.L. Drug delivery using composite scaffolds in the context of bone tissue engineering. Clinical Cases in Mineral and Bone Metabolism **10**, 155, 2013.

For Peer Review ONLY Not for Distribution

20. Inoda, H., Yamamoto, G., and Hattori, T. Histological investigation of osteoinductive properties of rh-BMP2 in a rat calvarial bone defect model. Journal of Cranio-Maxillofacial Surgery **32**, 365, 2004.

21. Chen, D., Zhao, M., and Mundy, G.R. Bone morphogenetic proteins. Growth factors **22**, 233, 2004.

22. G. dos S. Kotake, B., M. P. Salzedas, L., Ervolino, E., A. J. Calzzani, R., Sebald, W., and P. M. Issa, J. Bone Recuperation After rhBMP-2 Insertion in Alcoholic Animals-Experimental Study. Current Pharmaceutical Design **21**, 3557, 2015.

23. Siéssere, S., de Sousa, L.G., Issa, J.P.M., Iyomasa, M.M., Pitol, D.L., Barbosa, A.P.A., Semprini, M., Sebald, W., Bentley, M.V.B., and Regalo, S.C.H. Application of Low-Level Laser Irradiation (LLLI) and rhBMP-2 in Critical Bone Defect of Ovariectomized Rats: Histomorphometric Evaluation. Photomedicine and Laser Surgery **29**, 453, 2011.

24. Abdala, P.M.F., Iyomasa, M.M., Sato, S., Bentley, M.V.L.B., Pitol, D.L., Regalo, S.C.H., Siéssere, S., and Issa, J.P.M. Osteoinductivity potential of rhBMP-2 associated with two carriers in different dosages. Anatomical Science International **85**, 181, 2010.

25. Issa, J.P.M., do Nascimento, C., Bentley, M.V.L.B., Del Bel, E.A., Iyomasa, M.M., Sebald, W., and de Albuquerque Jr, R.F. Bone repair in rat mandible by rhBMP-2 associated with two carriers. Micron **39**, 373, 2008.

26. Haidar, Z.S., Hamdy, R.C., and Tabrizian, M. Delivery of recombinant bone morphogenetic proteins for bone regeneration and repair. Part A: Current challenges in BMP delivery. Biotechnology Letters **31**, 1817, 2009.

For Peer Review ONLY/ Not for Distribution

27. Schmidmaier, G., Schwabe, P., Strobel, C., and Wildemann, B. Carrier systems and application of growth factors in orthopaedics. Injury **39**, S37, 2008.

28. Girotti, A., Orbanic, D., Ibáñez-Fonseca, A., Gonzalez-Obeso, C., and Rodríguez-Cabello, J.C. Recombinant Technology in the Development of Materials and Systems for Soft-Tissue Repair. Advanced Healthcare Materials **4**, 2423, 2015.

29. Rodríguez-Cabello, J.C., Martín, L., Alonso, M., Arias, F.J., and Testera, A.M. "Recombinamers" as advanced materials for the post-oil age. Polymer **50**, 5159, 2009.

30. Urry, D.W. Molecular Machines: How Motion and Other Functions of Living Organisms Can Result from Reversible Chemical Changes. Angewandte Chemie International Edition in English **32**, 819, 1993.

31. Martin, L., Arias, F.J., Alonso, M., Garcia-Arevalo, C., and Rodriguez-Cabello, J.C. Rapid micropatterning by temperature-triggered reversible gelation of a recombinant smart elastin-like tetrablock-copolymer. Soft Matter **6**, 1121, 2010.

32. Ruoslahti, E., and Pierschbacher, M.D. Arg-Gly-Asp: a versatile cell recognition signal. Cell **44**, 517, 1986.

33. Lombard, C., Arzel, L., Bouchu, D., Wallach, J., and Saulnier, J. Human leukocyte elastase hydrolysis of peptides derived from human elastin exon 24. Biochimie **88**, 1915, 2006.

34. Goy, D.P., Gorosito, E., Costa, H.S., Mortarino, P., Pedemonte, N.A., Toledo, J., Mansur, H.S., Pereira, M.M., Battaglino, R., and Feldman, S. Hybrid matrix grafts to favor tissue regeneration in rabbit femur bone lesions. The open biomedical engineering journal **6**, 85, 2012.

For Peer Review ONLY/Not for Distribution

35. Coletta, D.J., Lozano, D., Rocha-Oliveira, A.A., Mortarino, P., Bumaguin, G.E., Vitelli, E., Vena, R., Missana, L., Jammal, M.V., Portal-Nunez, S., Pereira, M., Esbrit, P., and Feldman, S. Characterization of Hybrid Bioactive Glass-polyvinyl Alcohol Scaffolds Containing a PTHrP-derived Pentapeptide as Implants for Tissue Engineering Applications. The open biomedical engineering journal **8**, 20, 2014.

36. Rodríguez-Cabello, J.C., Girotti, A., Ribeiro, A., and Arias, F.J. Synthesis of Genetically Engineered Protein Polymers (Recombinamers) as an Example of Advanced Self-Assembled Smart Materials. In: Navarro M., Planell J.A., eds. Nanotechnology in Regenerative Medicine: Methods and Protocols. Totowa, NJ: Humana Press; 2012. pp. 17.

37. Orozco, L., Munar, A., Soler, R., Alberca, M., Soler, F., Huguet, M., Sentis, J., Sanchez, A., and Garcia-Sancho, J. Treatment of knee osteoarthritis with autologous mesenchymal stem cells: a pilot study. Transplantation **95**, 1535, 2013.

38. McKay, W.F., Peckham, S.M., and Badura, J.M. A comprehensive clinical review of recombinant human bone morphogenetic protein-2 (INFUSE® Bone Graft). International Orthopaedics **31**, 729, 2007.

39. Feldman, S., Cointry, G.R., Leite Duarte, M.a.E., Sarrió, L., Ferretti, J.L., and Capozza, R.F. Effects of hypophysectomy and recombinant human growth hormone on material and geometric properties and the pre- and post-yield behavior of femurs in young rats. Bone **34**, 203, 2004.

40. Meyer, D.E., and Chilkoti, A. Genetically Encoded Synthesis of Protein-Based Polymers with Precisely Specified Molecular Weight and Sequence by Recursive Directional Ligation: Examples from the Elastin-like Polypeptide System. Biomacromolecules **3**, 357, 2002.

For Peer Review ONLY / Not for Distribution

41. McPherson, D.T., Xu, J., and Urry, D.W. Product Purification by Reversible Phase Transition Following Escherichia coli Expression of Genes Encoding up to 251 Repeats of the Elastomeric Pentapeptide GVGVP. Protein Expression and Purification **7**, 51, 1996.

42. Fernandez-Colino, A., Arias, F.J., Alonso, M., and Rodriguez-Cabello, J.C. Self-organized ECM-mimetic model based on an amphiphilic multiblock silk-elastin-like corecombinamer with a concomitant dual physical gelation process. Biomacromolecules **15**, 3781, 2014.

43. Christensen, T., Hassouneh, W., Trabbic-Carlson, K., and Chilkoti, A. Predicting Transition Temperatures of Elastin-Like Polypeptide Fusion Proteins. Biomacromolecules **14**, 1514, 2013.

44. Ibáñez-Fonseca, A., Alonso, M., Arias, F.J., and Rodríguez-Cabello, J.C. Förster Resonance Energy Transfer-Paired Hydrogel Forming Silk-Elastin-Like Recombinamers by Recombinant Conjugation of Fluorescent Proteins. Bioconjugate Chemistry 2017.

45. Gibbs, D.M.R., Black, C.R.M., Dawson, J.I., and Oreffo, R.O.C. A review of hydrogel use in fracture healing and bone regeneration. Journal of tissue engineering and regenerative medicine **10**, 187, 2016.

46. Bessa, P.C., Machado, R., Nurnberger, S., Dopler, D., Banerjee, A., Cunha, A.M., Rodriguez-Cabello, J.C., Redl, H., van Griensven, M., Reis, R.L., and Casal, M. Thermoresponsive self-assembled elastin-based nanoparticles for delivery of BMPs. Journal of controlled release : official journal of the Controlled Release Society **142**, 312, 2010.

For Peer Review ONLY Not for Distribution

47. de Torre, I.G., Wolf, F., Santos, M., Rongen, L., Alonso, M., Jockenhoevel, S., Rodriguez-Cabello, J.C., and Mela, P. Elastin-like recombinamer-covered stents: Towards a fully biocompatible and non-thrombogenic device for cardiovascular diseases. Acta biomaterialia **12**, 146, 2015.

48. Pina, M.J., Girotti, A., Santos, M., Rodriguez-Cabello, J.C., and Arias, F.J. Biocompatible ELR-Based Polyplexes Coated with MUC1 Specific Aptamers and Targeted for Breast Cancer Gene Therapy. Molecular pharmaceutics **13**, 795, 2016.

49. Tomlinson, R.E., and Silva, M.J. Skeletal Blood Flow in Bone Repair and Maintenance. Bone Research **1**, 311, 2013.

50. Missana, L., Nagai, N., and Kuboki, Y. Comparative histological studies of bone and cartilage formations induced by various BMP-carrier composites. Journal of Oral Biosciences **36**, 9, 1994.

51. Issa, J.P.M., Defino, H.L.A., Netto, J.C., Volpon, J.B., Regalo, S.C.H., Iyomasa, M.M., Siéssere, S., and Tiossi, R. Evaluation of rhBMP-2 and Natural Latex as Potential Osteogenic Proteins in Critical Size Defects by Histomorphometric Methods. The Anatomical Record: Advances in Integrative Anatomy and Evolutionary Biology **293**, 794, 2010.

52. Issa, J.P.M., Do Nascimento, C., Lamano, T., Iyomasa, M.M., Sebald, W., and De Albuquerque Jr, R.F. Effect of recombinant human bone morphogenetic protein-2 on bone formation in the acute distraction osteogenesis of rat mandibles. Clinical Oral Implants Research **20**, 1286, 2009.

53. Hou, P., Troen, T., Ovejero, M.C., Kirkegaard, T., Andersen, T.L., Byrjalsen, I., Ferreras, M., Sato, T., Shapiro, S.D., Foged, N.T., and Delaissé, J.-M. Matrix

For Peer Review ONLY/Not for Distribution

metalloproteinase-12 (MMP-12) in osteoclasts: new lesson on the involvement of MMPs in bone resorption. Bone **34**, 37, 2004.

54. Taddese, S., Weiss, A.S., Jahreis, G., Neubert, R.H.H., and Schmelzer, C.E.H. In vitro degradation of human tropoelastin by MMP-12 and the generation of matrikines from domain 24. Matrix Biology **28**, 84, 2009.

55. Sallach, R.E., Cui, W., Balderrama, F., Martinez, A.W., Wen, J., Haller, C.A., Taylor, J.V., Wright, E.R., Long Jr, R.C., and Chaikof, E.L. Long-term biostability of self-assembling protein polymers in the absence of covalent crosslinking. Biomaterials **31**, 779, 2010.

56. Rodriguez-Cabello, J., Ribeiro, A., Reguera, J., Girotti, A., and Testera, A. 14 - Elastin-like systems for tissue engineering. Natural-Based Polymers for Biomedical Applications: Woodhead Publishing; 2008. pp. 374.

57. Tejeda-Montes, E., Klymov, A., Nejadnik, M.R., Alonso, M., Rodriguez-Cabello, J.C., Walboomers, X.F., and Mata, A. Mineralization and bone regeneration using a bioactive elastin-like recombinamer membrane. Biomaterials **35**, 8339, 2014.

58. Prieto, S., Shkilnyy, A., Rumplasch, C., Ribeiro, A., Arias, F.J., Rodríguez-Cabello, J.C., and Taubert, A. Biomimetic Calcium Phosphate Mineralization with Multifunctional Elastin-Like Recombinamers. Biomacromolecules **12**, 1480, 2011.

59. Vila, M., García, A., Girotti, A., Alonso, M., Rodríguez-Cabello, J.C., González-Vázquez, A., Planell, J.A., Engel, E., Buján, J., García-Honduvilla, N., and Vallet-Regí, M. 3D silicon doped hydroxyapatite scaffolds decorated with Elastin-like Recombinamers for bone regenerative medicine. Acta biomaterialia **45**, 349, 2016.

For Peer Review ONLY/Not for Distribution

60. Perez, R.A., Kim, J.-H., Buitrago, J.O., Wall, I.B., and Kim, H.-W. Novel therapeutic core–shell hydrogel scaffolds with sequential delivery of cobalt and bone morphogenetic protein-2 for synergistic bone regeneration. Acta biomaterialia **23**, 295, 2015.

61. Jo, S., Kim, S., Cho, T.H., Shin, E., Hwang, S.J., and Noh, I. Effects of recombinant human bone morphogenic protein-2 and human bone marrow-derived stromal cells on in vivo bone regeneration of chitosan–poly(ethylene oxide) hydrogel. Journal of Biomedical Materials Research Part A **101A**, 892, 2013.

62. Ren, Z., Wang, Y., Ma, S., Duan, S., Yang, X., Gao, P., Zhang, X., and Cai, Q. Effective Bone Regeneration Using Thermosensitive Poly(N-Isopropylacrylamide) Grafted Gelatin as Injectable Carrier for Bone Mesenchymal Stem Cells. ACS Applied Materials & Interfaces **7**, 19006, 2015.

63. Nguyen, T.B.L., and Lee, B.-T. A Combination of Biphasic Calcium Phosphate Scaffold with Hyaluronic Acid-Gelatin Hydrogel as a New Tool for Bone Regeneration. Tissue Engineering Part A **20**, 1993, 2014.

For Peer Review ONLY - Not for Distribution

For Peer Review ONLY, Not for Distribution

Figure Legends

FIG. 1. Molecular weight and purity assessment by SDS-PAGE and MALDI-TOF mass spectrometry for ELR-E-RGD and ELR-E-BMP2. MALDI-TOF spectra represent non-quantitative intensity (a.u.) against m/z (mass divided by net charge of the molecule) of the ELRs.

FIG. 2. SDS-PAGE images showing the biodegradation of the mixture of ELR-E-RGD (98%) and ELR-E-BMP-2 (2%) in solution at 1 mg/mL mediated by a) 1.2 U, b) 1.8 U and c) 2.4 U of elastase, at different sample collection times, as indicated above each picture (0, 10, 20, 30, 45, 60, 90 and 120 minutes after addition of the specific quantity of elastase). Picture d) shows the lack of elastase-mediated biodegradation in the case of the non-sensitive ELR. M represents the protein molecular weight marker.

FIG. 3. Graph showing the elastase-mediated cleavage rate of the highest molecular weight band with data obtained from analysis of the SDS-PAGE gels from Fig. 2. The net intensity of this double band at 113.6 and 107.8 kDa is represented at different sampling times.

FIG. 4. Graph showing hMSCs viability results after 3 days of culture in terms of cell number as measured using the Calcein AM assay for different ELR supplements in medium at 10 mg/mL: ELR-E-RGD (represented as RGD), ELR-E-BMP-2 (BMP-2), the mixture of both (98% (w/w) ELR-E-RGD and 2% (w/w) ELR-E-BMP-2, RGD/BMP-2) and supplement-free medium (medium only). No significant differences ($p > 0.05$) were found in any case.

FIG. 5. Graph showing the number of hMSCs attached to the ELR-coated well-plates as measured using the Calcein AM assay for different ELR coatings absorbed at 5 mg/mL:

ELR-E-RGD (represented as RGD), ELR-E-BMP-2 (BMP-2), the mixture of both (98% (w/w) ELR-E-RGD and 2% (w/w) ELR-E-BMP-2, RGD/BMP-2) and non-coated tissue culture plates (TCP) (n = 4). (*) $p < 0.05$, (**) $p < 0.01$.

FIG. 6. a) Axial computed tomography of right rabbit femora showing full cortical medial regeneration in six out of seven samples. The fourth sample from the left shows persistence in the cortical defect at the injury site (white arrow). b) Axial computed tomography of right rabbit femora showing a coronal slice of the samples. From left to right, in the fourth sample, the persistence of a cortical defect approximately 1 mm in size can be observed in the distal metaphysis (white arrow). c) Medial view of the 3D reconstruction of a rabbit right femur. The restitution of cortical bone at the distal metaphysis can be observed (black circumference). d) Medial view of the 3D reconstruction of a rabbit right femur. In this case, the sample with the remaining partial defect shows a small hollow with continuity (white arrow).

FIG. 7. Microphotographs taken from decalcified femoral bone sections stained with hematoxylin and eosin. a) Thick lamellar bone showing numerous vascular blood channels (black asterisk), remnants of the ELR hydrogel (blue asterisk), hematopoietic bone marrow and osteoblast layers (green asterisk) are observed in the EFI region. Magnification 46.6x, bar = 1 mm. b) The high magnification images show the interface between new lamellar bone (black asterisk) and the ELR hydrogel (red asterisk), with a network aspect acting as a guide for cells. Magnification 233.4x, bar = 500 μm. c) At high magnification, a few vascular channels are observed in new lamellar bone at the EFI. Each layer of bone is deposited in the form of a "mosaic pattern", resembling pagetoid-like bone. Magnification 700.2x, bar= 250 μm. d) At high magnification the ELR hydrogel shows mineralized amorphous regions surrounded by osteoblast-like cells (black arrows). Micro-hemorrhage (red asterisk) and congestive vessels (grey

For Peer Review ONLY / Not for Distribution

asterisk) are also observed. Magnification 700.2x bar= 250 μm. e) At low magnification, a panoramic microphotography of the femoral epiphysis and metaphysis shows new bone formed in the EFI region (black asterisk). This bone is surrounded by hematopoietic bone marrow (green asterisk) with a few trabeculae (orange asterisk). Magnification 80x, bar = 2 mm. f) A few bone nodules surrounding the EFI region are lined by several layers of prominent osteoblasts (black arrows). Osteocytes (green arrows) are observed inside a nodule. Magnification 700.2x, bar = 250 μm.

For Peer Review ONLY/ Not for Distribution

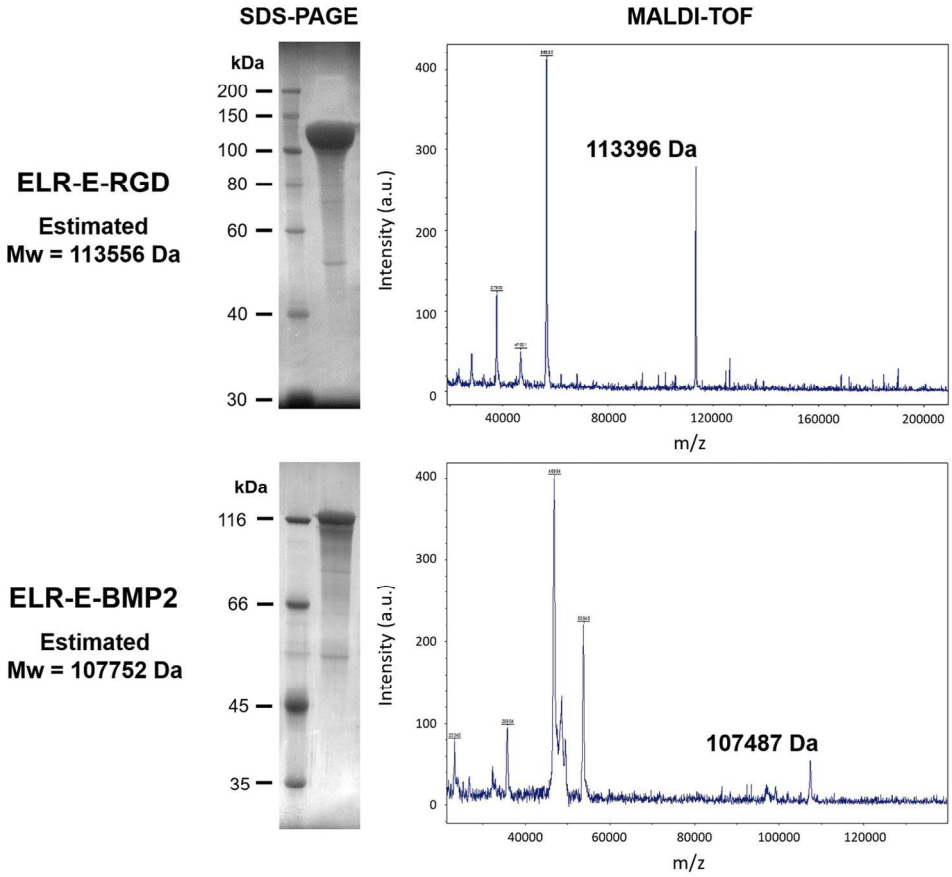

150x135mm (300 x 300 DPI)

For Review - for Distribution

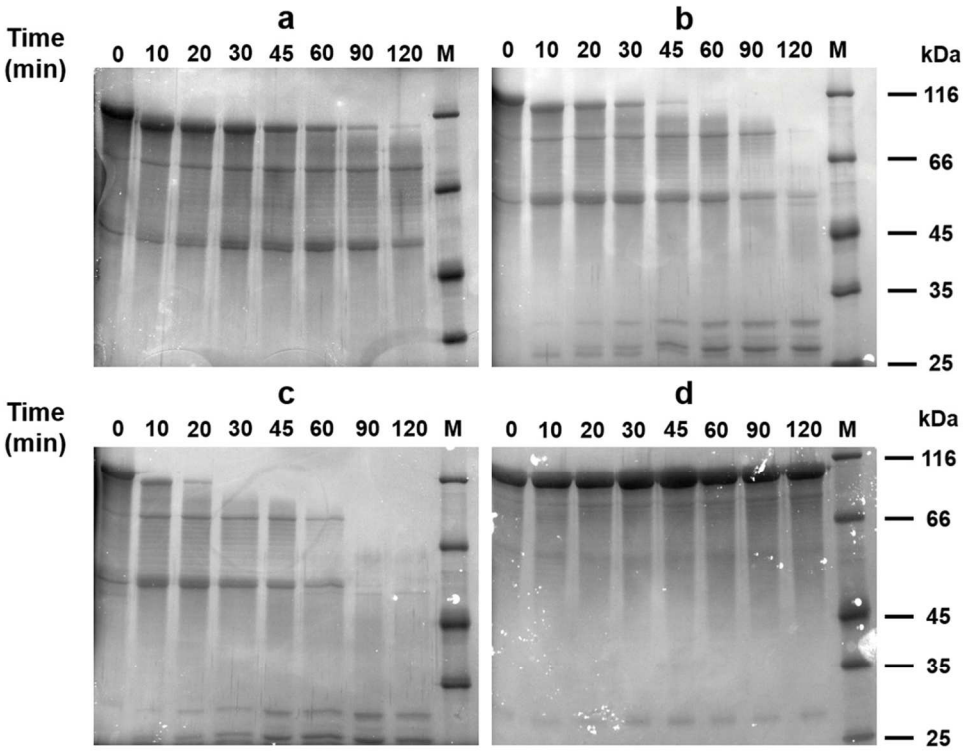

150x117mm (300 x 300 DPI)

For Review Not for Distribution

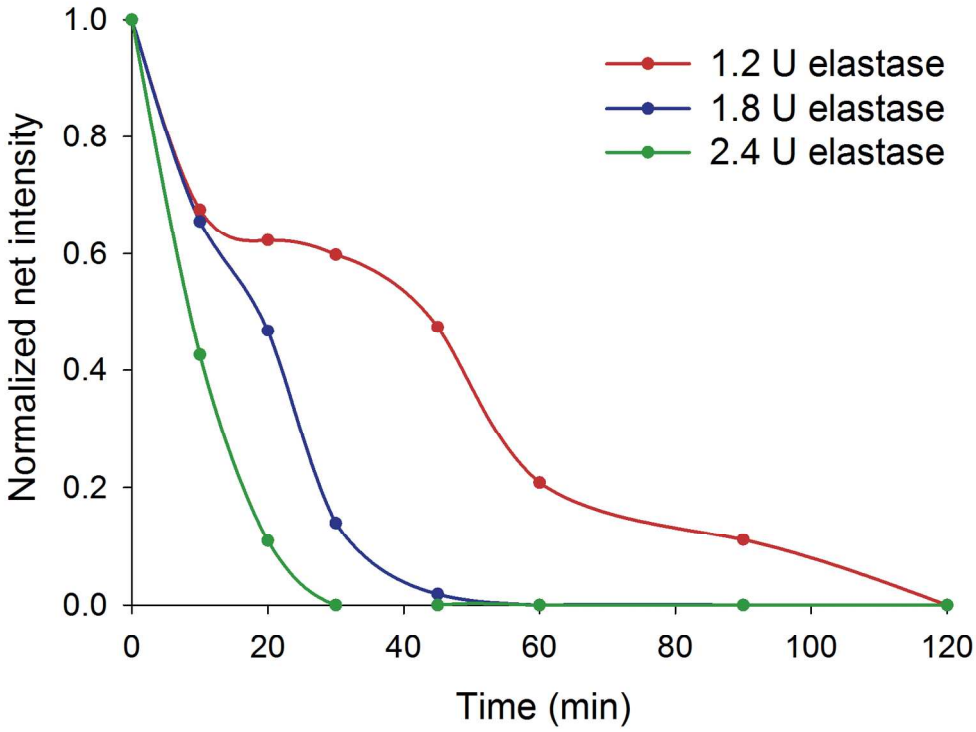

153x123mm (300 x 300 DPI)

For Review Not for Distribution

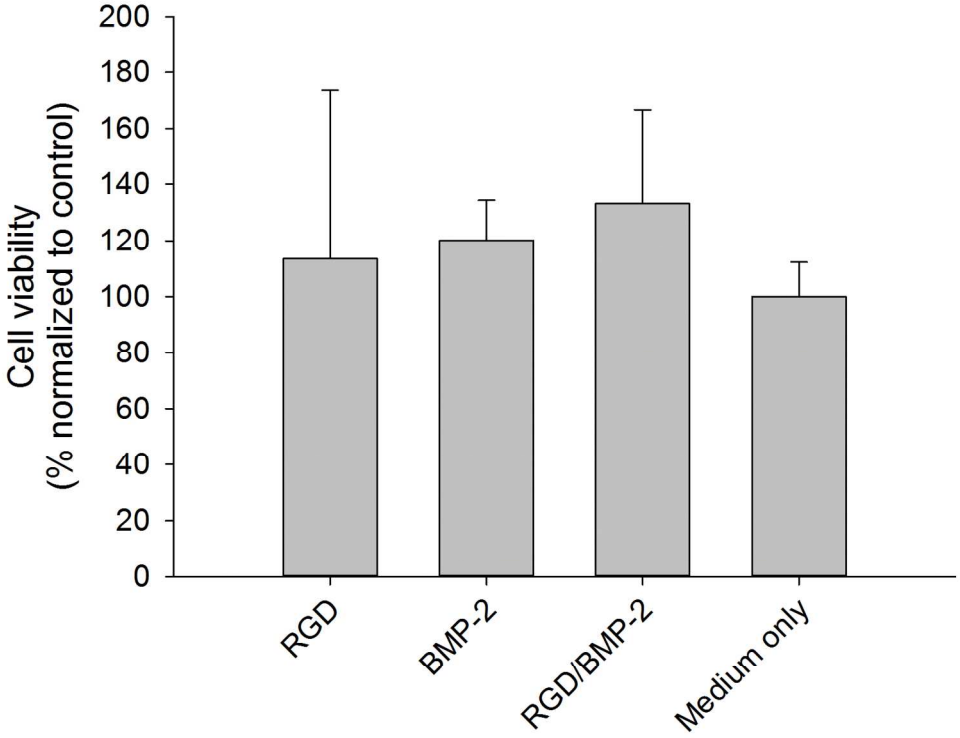

149x125mm (300 x 300 DPI)

For Review Only
Not for Distribution

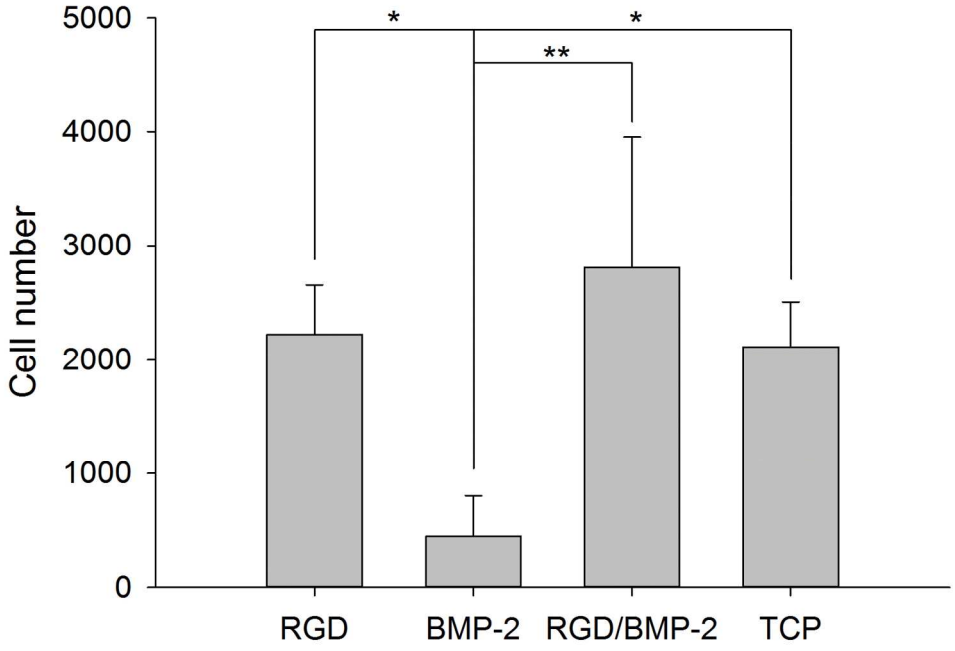

149x110mm (300 x 300 DPI)

For Review Not for Distribution

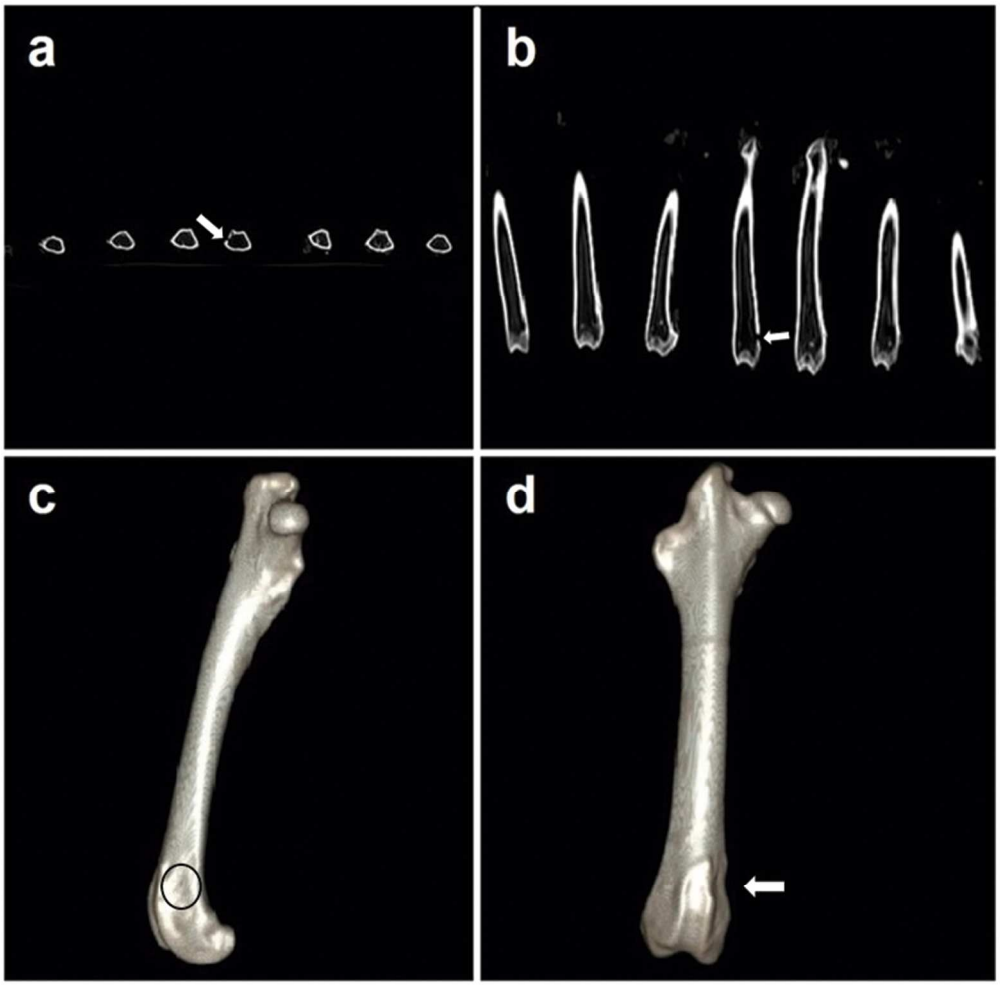

147x145mm (300 x 300 DPI)

For Review Only

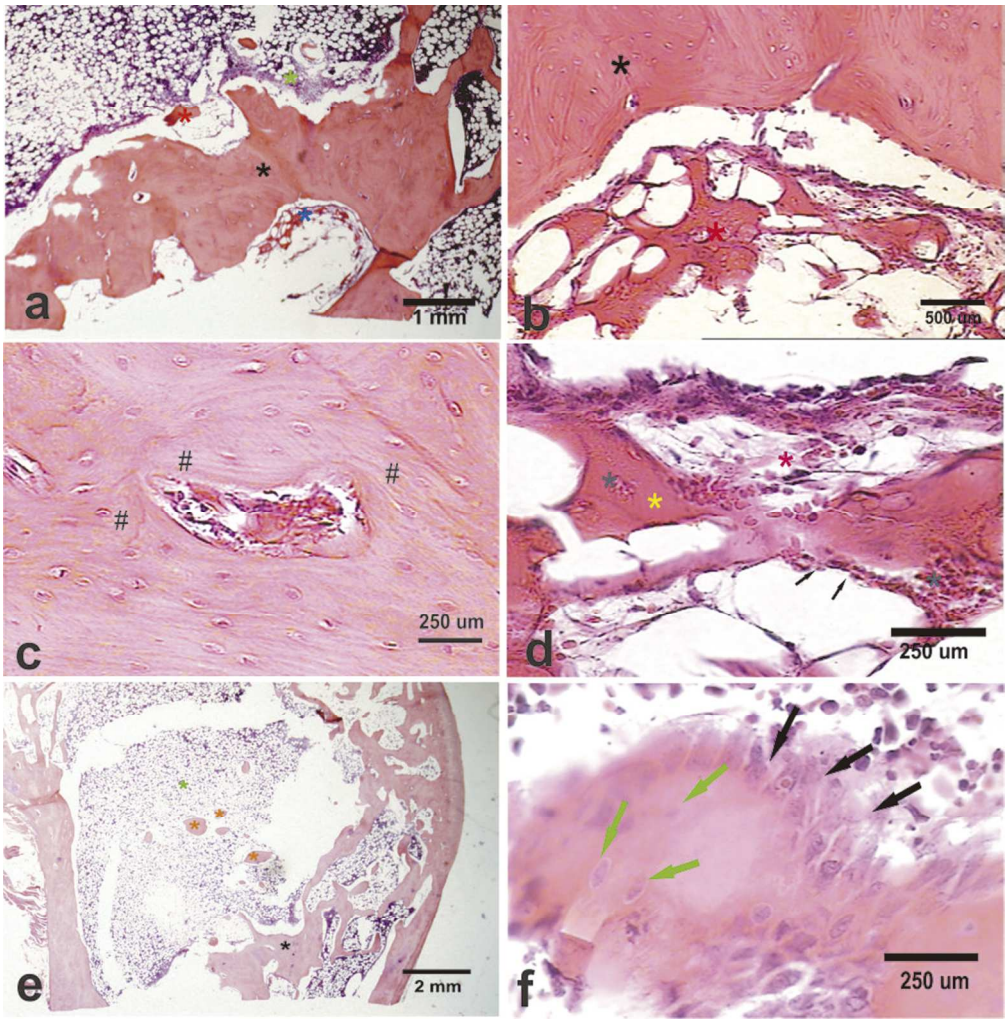

150x151mm (300 x 300 DPI)

Supplementary Information

Bone regeneration mediated by a bioactive and biodegradable ECM-like hydrogel based on elastin-like recombinamers

Dante J. Coletta, MD,[1#] Arturo Ibáñez-Fonseca, MSc,[2#] Liliana R. Missana, PhD,[3,4#] María V. Jammal, PhD,[3,4] Ezequiel J. Vitelli, MD,[1] Mariangeles Aimone, BSc,[1] Facundo Zabalza, BSc,[1] João P. Mardegan Issa, PhD,[5] Matilde Alonso, PhD,[2] José Carlos Rodríguez-Cabello, PhD,[2] and Sara Feldman, PhD,[1]

[#] These authors contributed equally to this work.

[1] LABOATEM. Osteoarticular Biology, Tissue Engineering and Emerging Therapies Laboratory, School of Medicine, National Rosario University, Rosario, Argentina.

[2] BIOFORGE Lab, University of Valladolid, CIBER-BBN, Valladolid, Spain.

[3] Experimental Pathology & Tissue Engineering Laboratory, Dental School, National Tucumán University, Tucumán, Argentina.

[4] Tissues Laboratory, Proimi-Biotechnology-Conicet, Tucumán, Argentina.

[5] Ribeirão Preto School of Dentistry, University of São Paulo, São Paulo, Brazil.

For Peer Review Only - Not for Distribution

For Peer Review ONLY/ Not for Distribution

Supplementary Methods

ELR biosynthesis and characterization

The block co-polymer that constitutes the ELR backbone was designed to comprise a hydrophobic block (containing isoleucine as the guest residue), known as I_{60}, which is able to establish physical interactions above the T_t, i.e. at physiological temperature. Moreover, it includes a hydrophilic block (containing glutamic acid with a carboxylic group), termed E_{50}, which remains hydrated at physiological temperature. Both the ELRs designed and used in this work include an elastase cleavage sequence for biodegradation, as described above. One of them was genetically engineered to include a RGD domain for cell attachment, while the other one included the BMP-2 domain to enhance osteogenesis, thus giving ELR-Elastase-RGD (ELR-E-RGD) and ELR-Elastase-BMP-2, respectively (Fig. S1, Supplementary Information).

The mechanical properties of the hydrogels formed by the ELRs above the T_t were assessed by rheological testing in a controlled stress rheometer (AR2000ex, TA Instruments) equipped with a Peltier plate for control of the temperature and a 12 mm plate diameter for the shear stress. To that end, a mixture of both ELRs (98% (w/w) ELR-E-RGD and 2% (w/w) ELR-E-BMP-2, see below) was dissolved in PBS at 300 mg/mL and 4 ºC for 24 h. Hydrogels were then formed *in situ* by depositing 200 μL of the solution onto the cold Peltier plate and increasing the temperature to 37 ºC. Time sweep experiments were conducted at a constant strain of 0.5% and a frequency of 1 Hz.

Elastase-mediated cleavage of the ELR in solution

SDS-PAGE was performed to evaluate the biodegradation of the samples incubated with elastase, comparing those taken at different time points with the original sample at the beginning of the experiment. Gels were prepared at a polyacrylamide (Acryl/Bis™, Amresco, USA) concentration of 10%. The protein molecular weight marker used was Pierce Unstained Protein MW Marker (Thermo Fisher, USA). Images were obtained using the Gel Logic 100 Imaging System (Eastman Kodak, USA) and analyzed using Kodak 1D Image Analysis software (Eastman Kodak, USA).

In vivo *experiments*

Pre-surgical preparation

Antibiotic prophylaxis was carried out prior to the surgical procedure by applying cefazolin at a dose of 50 mg/kg/day, administered intramuscularly.

The anesthetic treatment was performed by combining three drugs, which were administered intramuscularly, namely Ketamine Hydrochloride at 35 mg/kg/day, Xylazine Hydrochloride (2.0%) at 18 mg/kg, and Acepromazine Maleate (1.0%) at 1 mg/kg, achieving complete relaxation of the animal. This anesthetic effect lasted for 45-60 minutes.

Surgical procedure

The area was shaved with an electric shaver, brushed with a 10% povidone-iodine solution, and immediately covered with fenestrated drapes. The intervention began with a longitudinal cutaneous incision of 4 cm in the internal lateral distal metaphysis of the femur, immediately above the medial condyle.

For Peer Review ONLY / Not for Distribution

Both the medial and lateral flaps were separated, and a non-muscular aponeurotic plane was opened until the desired bone area had been reached through the divulsion in said tissues. The central point of the perforation was marked with a bradawl, and the first hole was cut immediately, using a drill with a 3 mm diameter bit attached to a sterile electric motor. Milling was subsequently continued using a 6 mm diameter bit to obtain the desired bone defect of no more than 3 mm in depth. The bone defect was washed with a sterile physiological solution to eliminate detritus, and hemostasis of the lesion was performed using a sterile swab plus gauze. The area was then dried with a sterile gauze and filled with the chilled ELR solution to form a hydrogel *in situ*. To this end, 100 μL of the solution was placed into the hole created in the bone using an automatic pipette and sterile tips, which were stored at 4 ºC to avoid gelification of the ELR before and during implantation. The aponeurotic plane was first sutured using resorbable material type 3/0, then the skin was sutured with 3/0 Nylon, and disinfected with povidone-iodine.

Post-surgical clinical studies

During the study period, the overall status, mobility and food intake of the animals were monitored daily. Body temperature was measured daily during the first week, and then weekly thereafter. Biochemical parameters (complete blood count) were evaluated using standard procedures at days 0, 2, 30 and at the end of the study. Total serum proteins, albumin, alanine aminotransferase (ALT) and aspartate aminotransferase (AST) were evaluated using standard commercial kits (Wiener lab Group, Argentina) (data not shown).

For Peer Review ONLY/ Not for Distribution

Supplementary Figures and Tables

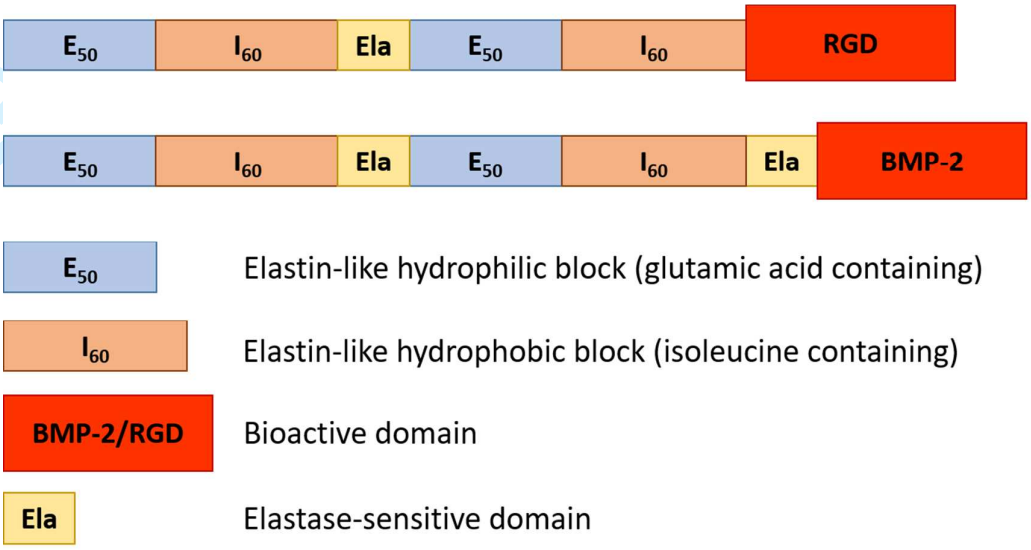

FIG. S1. Original scheme of the design of the ELRs engineered for this work, ELR-E-RGD and ELR-E-BMP-2, respectively.

For Peer ONLY/ Not for Distribution

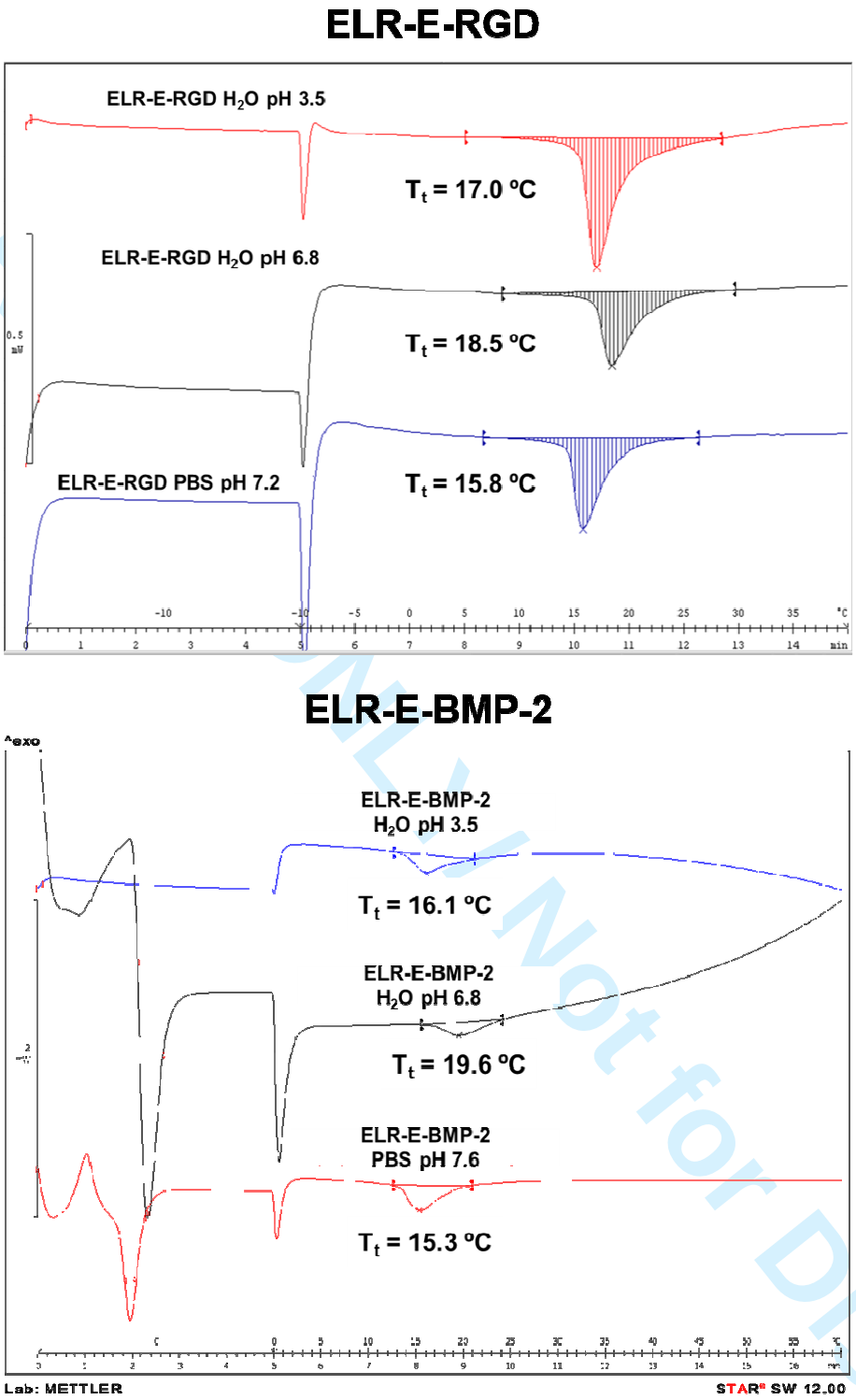

FIG. S2. DSC graphs of ELR-E-RGD (top) and ELR-E-BMP-2 (bottom) showing the T_t of both ELRs in different solvents (water and PBS) and at different pH values.

For Peer Review Only - Not for Distribution

TABLE S1. Comparison between the predicted number of each amino acid in ELR-E-RGD and the experimental values.

Amino acid	Predicted	Experimental
ASP+ASN	2+0	2.47
GLU+GLN	21	25.54
SER	7	5.34
HIS	-	-
GLY	530	533.99
THR	2	2.30
ARG	2	1.13
ALA	7	6.01
TYR	-	-
CYS	-	-
VAL	350	344.22
MET	1	0.66
TRP	-	-
PHE	-	-
ILE	160	158.98
LEU	2	2.32
LYS	-	-
PRO	266	267.47

For Peer Review ONLY/ Not for Distribution

TABLE S2. Comparison between the predicted number of each amino acid in ELR-E-BMP-2 and the experimental values.

Amino acid	Predicted	Experimental
ASP+ASN	6+7	10.30
GLU+GLN	26+2	34.82
SER	9	6.54
HIS	5	3.38
GLY	457	463.15
THR	3	3.01
ARG	2	5.79
ALA	12	14.94
TYR	5	8.43
CYS	7	7.32
VAL	325	313.03
MET	3	2.31
TRP	2	-
PHE	3	2.92
ILE	124	121.54
LEU	10	10.29
LYS	6	3.74
PRO	234	233.16

For Peer Review ONLY/ Not for Distribution

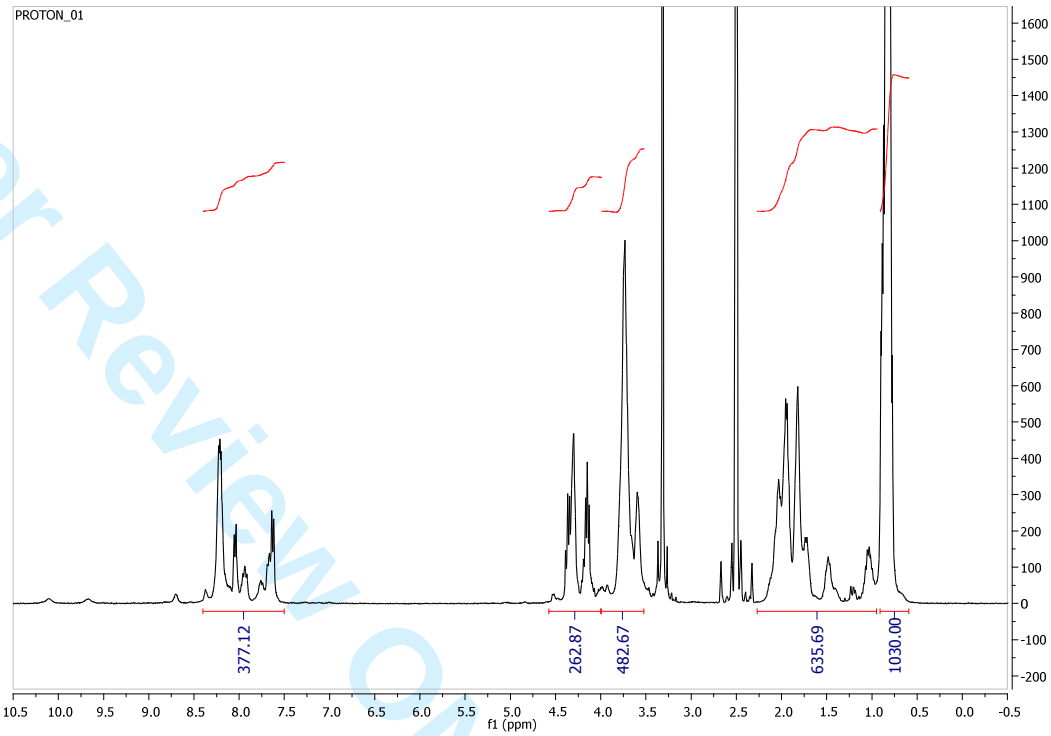

FIG. S3. H-NMR spectrum of ELR-E-RGD showing the integration of the peaks corresponding to the different types of hydrogens.

TABLE S3. Comparison between the predicted value of each type of hydrogen in ELR-E-RGD and the experimental values found by integration of each peak in the corresponding H-NMR spectrum.

Type of hydrogen	Predicted value	Measured value
$-C\underline{H}_3$	1030	Reference
$-C\underline{H}-$ and $-C\underline{H}_2-$	1475	1381.2
$-N\underline{H}_2$	363	377.1

For Peer Review ONLY / Not for Distribution

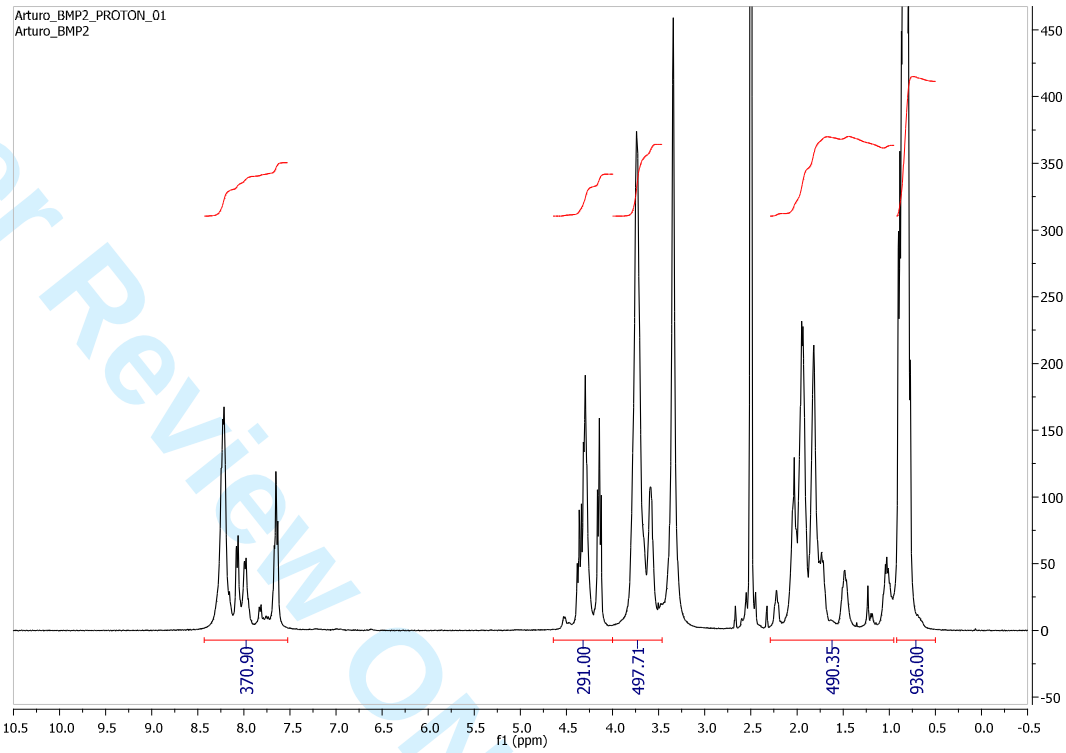

FIG. S4. H-NMR spectrum of ELR-E-BMP-2 showing the integration of the peaks corresponding to the different types of hydrogens.

TABLE S4. Comparison between the predicted value of each type of hydrogen in ELR-E-BMP-2 and the experimental values found by integration of each peak in the corresponding H-NMR spectrum.

Type of hydrogen	Predicted value	Measured value
$-C\underline{H}_3$	936	Reference
$-C\underline{H}-$ and $-C\underline{H}_2-$	1370	1279.1
$-N\underline{H}_2$	355	370.9

For Peer Review ONLY/ Not for Distribution

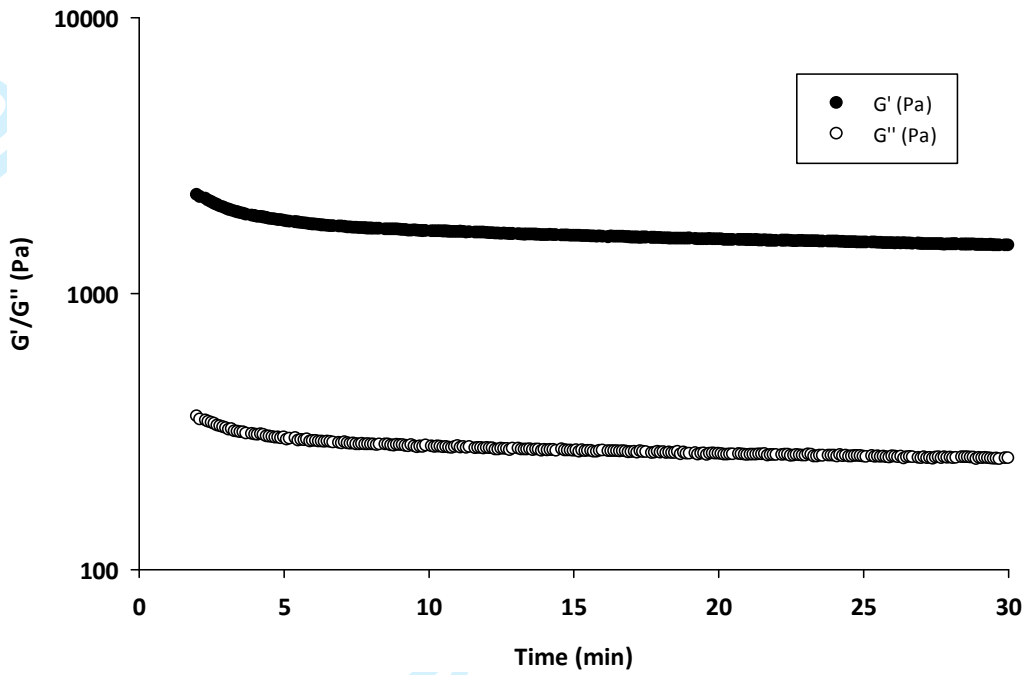

FIG. S5. Graph showing the mechanical properties of a hydrogel made of a mixture of ELR-E-RGD (98% (w/w)) and ELR-E-BMP-2 (2% (w/w)) at 300 mg/mL in PBS.

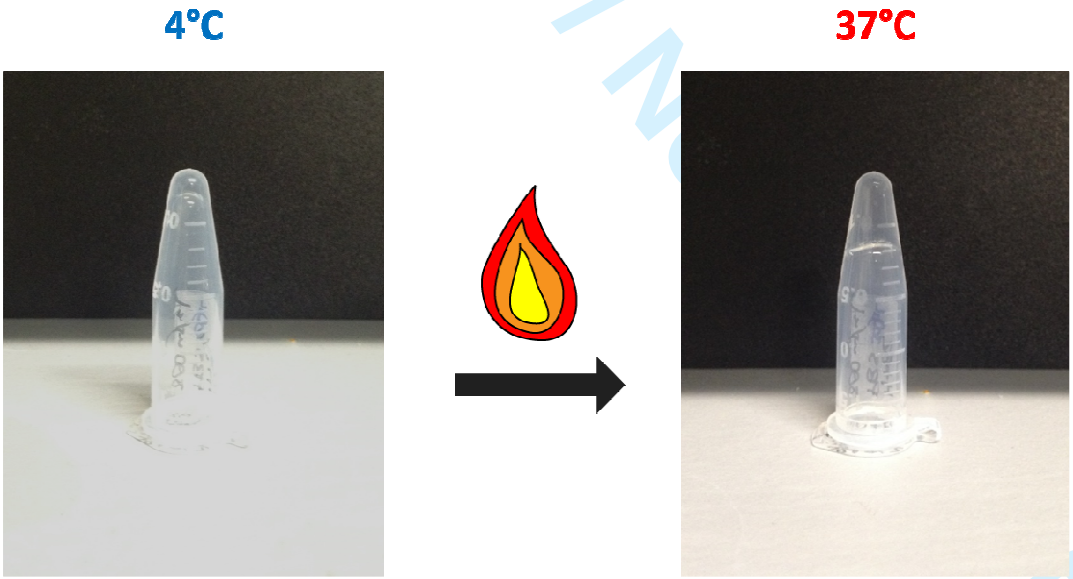

FIG. S6. Hydrogel formation due to a temperature increase above the T_t of a mixture of ELR-E-RGD (98% (w/w)) and ELR-E-BMP-2 (2% (w/w)) at 300 mg/mL in PBS. The

For Peer Review Only/ Not for Distribution

solution was first kept in an ice bath until complete dissolution. Then, it was incubated at 37ºC for 5 minutes to allow the formation of the hydrogel.

TABLE S5. Table showing the expected molecular weight, the molecular weight plus 20%, and the calculated (experimental) *Mw* of the bands appearing upon elastase-mediated degradation.

Nascent bands	**Expected *Mw* (kDa)**	**Expected *Mw* + 20% (kDa)**	**Calculated *Mw* (kDa)**
Nascent band 1	66.5-65.5	79.8-78.6	80.8
Nascent band 2	48.2-46.7	57.8-56.0	54.2

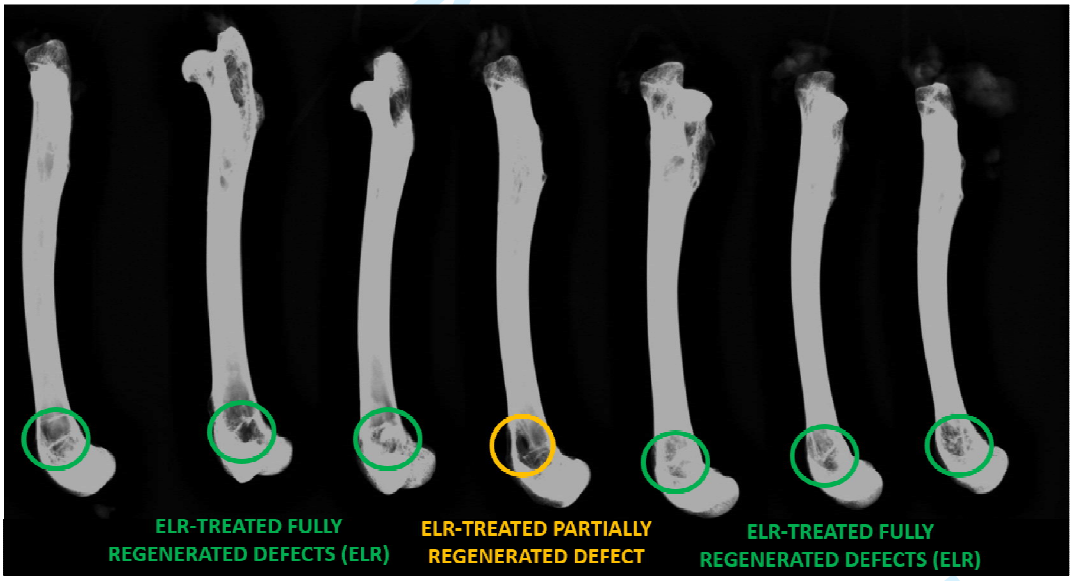

FIG. S7. Radiography showing the seven femora extracted at the end of the experiment. Green circles correspond to fully regenerated defects (six out of seven samples) and the yellow circle to a partially regenerated defect.

For Peer Review Only Distribution